Nonlinear coherent structures of Alfvén wave in a collisional plasma

Sayanee Jana, Samiran Ghosh, and Nikhil Chakrabarti

Citation: Phys. Plasmas **23**, 072304 (2016); doi: 10.1063/1.4958651
View online: http://dx.doi.org/10.1063/1.4958651
View Table of Contents: http://aip.scitation.org/toc/php/23/7
Published by the American Institute of Physics

Nonlinear coherent structures of Alfvén wave in a collisional plasma

Sayanee Jana,[1] Samiran Ghosh,[2] and Nikhil Chakrabarti[3]
[1]Saha Institute of Nuclear Physics, 1/AF Bidhannagar, Kolkata 700 064, India
[2]Department of Applied Mathematics, University of Calcutta, 92, Acharya Prafulla Chandra Road, Kolkata 700 009, India
[3]Saha Institute of Nuclear Physics, 1/AF Bidhannagar, Kolkata 700 064, India

(Received 13 April 2016; accepted 28 June 2016; published online 15 July 2016)

The Alfvén wave dynamics is investigated in the framework of two-fluid approach in a compressible collisional magnetized plasma. In the finite amplitude limit, the dynamics of the nonlinear Alfvén wave is found to be governed by a modified Korteweg-de Vries Burgers equation (mKdVB). In this mKdVB equation, the electron inertia is found to act as a source of dispersion, and the electron-ion collision serves as a dissipation. The collisional dissipation is eventually responsible for the Burgers term in mKdVB equation. In the long wavelength limit, this weakly nonlinear Alfvén wave is shown to be governed by a damped nonlinear Schrödinger equation. Furthermore, these nonlinear equations are analyzed by means of analytical calculation and numerical simulation to elucidate the various aspects of the phase-space dynamics of the nonlinear wave. Results reveal that nonlinear Alfvén wave exhibits the dissipation mediated shock, envelope, and breather like structures. Numerical simulations also predict the formation of dissipative Alfvénic rogue wave, giant breathers, and rogue wave holes. These results are discussed in the context of the space plasma. *Published by AIP Publishing.* [http://dx.doi.org/10.1063/1.4958651]

I. INTRODUCTION

Low-frequency magneto-hydrodynamic waves (MHD),[1,2] in general, and Alfvén waves, in particular, are ubiquitous in the laboratory[3] and space plasma.[4] Among these low-frequency waves, nonlinear Alfvén waves have been a topic of intense research work to the plasma physics community because of its applications in various physical processes related to particle energization in magnetized plasma,[5] self-modulation in strongly magnetized plasma,[6] tokamak plasma heating,[7] and interplanetary shocks.[8] In 1988, Kennel *et al.*, in their pioneering work,[9] have shown that in the absence of any dissipation, competition between the wave nonlinearity and dispersion leads to the appearance of Alfvénic soliton in which wave dispersion arises due to coupling of the elliptically polarized magnetic field component in a two-dimensional electron-ion plasma. In the weak amplitude limit, the dynamics of the low-frequency dispersive Alfvén wave is governed by the well-known Korteweg-de Vries (KdV) equation, whereas a modified KdV (mKdV) equation governs the dynamics of the nonlinear intermediate frequency wave.[9] In the presence of Hall effects, in the limit of wavelengths much larger than the ion inertial length, the dynamics of the nonlinear Alfvén wave propagating along a direction either parallel or making a small angle with the magnetic field is governed by a derivative, nonlinear Schrödinger equation (DNLSE), which describes Alfvénic soliton and Alfvén wave turbulence.[9,10]

Moreover, the MHD waves are highly dissipative,[11] and the dissipation leads to the coronal heating in solar physics. The Alfvén wave is thought to be a possible candidate for solar corona heating as it can transport energy fluxes over a large distance. The resonant absorption and plasma heating enhance the chance of dissipation (via viscosity and/or resistivity) that leads to the Alfvén wave heating.[12,13] In recent past, various nonlinear phenomena of Alfvén waves from the kinetic to inertial regime have been established by means of numerous laboratory observations as well as theoretical analysis.[14–20] Nonlinear phenomena of Alfvén waves in low beta plasmas now become a very important research area to the plasma physicists.[21] In 2011, Laveder *et al.*[22] reported for the first time about the generation of freak waves or rogue waves in the context of strong Alfvén wave turbulence in a plasma taking two-component magnetic field into consideration. In contrast, considering one component magnetic field, we report here the formation of dissipative rogue waves, giant breathers, and rogue wave holes in the context of the weakly nonlinear, dispersive Alfvén wave in a collisional electron-ion plasma.

In the present work, we have investigated the dynamics of the linearly polarized, weakly nonlinear Alfvén wave in the framework of Lagrangian two-fluid theory in a cold plasma[23–26] in the presence of finite electron inertia effect. The electron-ion collision induced dissipative effects are also taken into account. Interestingly, the effect of finite electron inertia acts as a source of wave dispersion. In the quasi-linear limit, the dynamics of the nonlinear Alfvén mode is shown to be governed by a modified Korteweg-de Vries Burgers (mKdVB) equation, where the electron-ion collision is responsible for the Burgers term, and as mentioned before, the electron inertia is responsible for the dispersive term. In the long-wavelength limit, we have also investigated another important physical phenomenon known as the modulational instability. A slow parallel modulation of a finite amplitude low-frequency Alfvén wave can grow and, in some limit, leads to the formation of a bright (envelope) soliton. The physics behind this modulational instability is the interplay

between nonlinearity and dispersion due to the finite electron inertia. The nonlinearity mainly originates from the ponderomotive force. The dynamics of this modulated wave is shown to be described by a nonlinear Schrödinger equation (NLSE) with a linear damping term arising due to electron-ion collision. These two nonlinear equations (mKdVB and NLSE) are analyzed by means of analytic calculation and numerical simulation. Both the results reveal that the nonlinear Alfvén wave exhibits dispersive (when dispersion dominates over dissipation) and monotonic (when dissipation dominates over dispersion) shocks, dissipative envelope, and breathers. Numerical simulations also predict the formation of rogue or freak waves, giant breathers, and rogue wave holes which are highly localized phenomenon in both space and time.[27–31] The rogue waves and breathers are observed experimentally in nonlinear fibre optics,[32] water waves,[33,34] in multi-component plasma[35] and in strong Alfvén wave turbulence.[22] Recently, the rogue wave holes are observed experimentally in water waves[36] and multi-component plasma.[37] However, the results of this investigation show that similar structures are also spontaneously generated in the context of the weakly nonlinear Alfvén wave in an electron-ion plasma. Therefore, all the results are not only valid in plasmas but also in many other cross disciplinary field of physics. Moreover, the present investigation shows that it is not necessary to consider two-component magnetic field to describe the nonlinear and dispersive Alfvén wave in electron-ion plasma. One component is sufficient to describe the essential features of nonlinear, dispersive Alfvén wave, where the electron mass provides the dispersive effect. However, two-component magnetic field might lead to some other important aspects of Alfvén wave, which will be considered in future investigation.

The paper is organized as follows: The governing equations in the Lagrangian fluid variables are derived in Sec. II. The small amplitude nonlinear dynamics of the Alfvén wave described by an mKdVB equation and its nonlinear analysis are studied in Sec. III. In Sec. IV, we have investigated the wave modulational characteristic of the nonlinear wave governed by a damped NLSE. The numerical simulation of the nonlinear equations and the results are discussed in Sec. V. Finally in Sec. VI, we have given a summary and brief discussion of the results of the present investigation.

II. BASIC EQUATIONS

We consider first the two-fluid model of a cold plasma, in which each distinct species of particle is specified by the index α, with mass m_α, and charge q_α. Each collection of particles of a specific type is supposed to act as a fluid, with its own velocity U_α and number density n_α. Each fluid is collision dominated and acted on by the electric and magnetic fields and may act on the other fluids via collisions. We also assume low-β_p plasma (where $\beta_p = 8\pi nT/B_0^2 (\ll 1)$, n is the plasma density, T is the plasma temperature, and B_0 is the strength of the magnetic field), so that the cold plasma approximation is justified.[38] The uniform external magnetic field is in the $\hat{e}_x$ direction ($B_0\hat{e}_x$). To investigate the dynamics of the nonlinear Alfvén wave propagating in the direction of the external magnetic field, we consider the equation of motion for the fluid corresponding to the species α

$$m_\alpha n_\alpha \left(\frac{\partial}{\partial t} + \mathbf{U}_\alpha \cdot \nabla\right)\mathbf{U}_\alpha = n_\alpha q_\alpha \left(\mathbf{E} + \frac{1}{c}\mathbf{U}_\alpha \times \mathbf{B}\right) + m_\alpha n_\alpha \nu_{\alpha\beta}(\mathbf{U}_\beta - \mathbf{U}_\alpha), \quad (1)$$

where $\nu_{\alpha\beta}$ is the collision frequency of particle of species α with particles of species β. In this work, we consider only electron ion plasma ($\alpha \equiv e, i$) in which $q_e \equiv -e$ and $q_i = e$, where e is the fundamental unit of electronic charge.

The continuity equation for each fluid is

$$\frac{\partial n_\alpha}{\partial t} + \nabla \cdot (n_\alpha \mathbf{U}_\alpha) = 0 \quad (2)$$

and the following Maxwell's equations are

$$\nabla \times \mathbf{E} = -\frac{1}{c}\frac{\partial \mathbf{B}}{\partial t}, \quad (3)$$

$$\nabla \times \mathbf{B} = \frac{4\pi \mathbf{J}}{c} = \frac{4\pi}{c} q_\alpha n_\alpha U_\alpha, \quad (4)$$

where summation convention is used. All symbols have their usual meaning. In this work, we are interested in the low-frequency mode ($\omega \ll \omega_{pe}$, electron plasma frequency), so that we neglect the displacement current compared to particle current in Eq. (4). To describe the Alfvén wave, we assume that all the dynamical variables are functions of x and t. The low frequency assumption is also consistent with the quasi-neutrality condition $n_i \approx n_e \equiv n$. On the basis of the above facts, from the continuity equations for both species (Eq. (2)), we obtain

$$\frac{\partial}{\partial x}[n(U_{ix} - U_{ex})] = 0 \Rightarrow U_{ix} = U_{ex} = u\,(\text{say}), \quad (5)$$

where we assume that $U_{ix}(0,t) = U_{ex}(0,t) = 0$.

In the Alfvén wave dynamics, the perturbed magnetic field B arises from the spatial variation of polarization current and directed along the z-direction. In component form, Eq. (4) can be written as

$$\frac{\partial B}{\partial x} = -\frac{4\pi en}{c}(U_{iy} - U_{ey}), \quad (6)$$

$$0 = \frac{4\pi en}{c}(U_{iz} - U_{ez}). \quad (7)$$

Equation (6) implies that the conduction current flows along y (the direction perpendicular to the plasma motion). From Eq. (7), we find $U_{iz} = U_{ez} = v\,(\text{say})$ In view of these continuity equations, we have

$$\left(\frac{\partial}{\partial t} + u\frac{\partial}{\partial x}\right)n = -n\frac{\partial u}{\partial x}, \quad (8)$$

whereas momentum equations (1) can be written separately for electrons and ions as

$$m_e\left(\frac{\partial}{\partial t} + u\frac{\partial}{\partial x}\right)\mathbf{U}_e = -e\left(\mathbf{E} + \frac{1}{c}\mathbf{U_e} \times \mathbf{B}\right) + m_e\nu_{ei}(\mathbf{U}_i - \mathbf{U}_e), \quad (9)$$

$$m_i\left(\frac{\partial}{\partial t}+u\frac{\partial}{\partial x}\right)\mathbf{U}_i = e\left(\mathbf{E}+\frac{1}{c}\mathbf{U}_i\times\mathbf{B}\right)+m_i\nu_{ie}(\mathbf{U}_e-\mathbf{U}_i). \tag{10}$$

Equations (8)–(10) have a symmetry in the convective operator. This nonlinear operator may be simplified by introducing the Lagrangian variables $(\xi,\ \tau)$ through the following transformation:

$$\xi = x-\int_0^\tau u(\xi,\tau')d\tau', \quad \tau = t. \tag{11}$$

With this transformation, the derivative operators are transformed accordingly similar to Ref. 26. Using these transformations, the continuity equation (8) is simplified and expressed as $n(\xi,\tau)/n(\xi,0)=\partial\xi/\partial x$. Noticed that the work in Ref. 26 deals with the magnetosonic wave dynamics that propagates perpendicular to the magnetic field. In contrast to that work, here we investigate the dynamics of the Alfvén wave which propagates along the magnetic field. One can easily observe that the equations in both situations although look similar but there are substantial difference in their character. Due to the presence of equilibrium magnetic field in the derivation of Alfvén wave, we have one extra degree of freedom which reflects in an extra equation (19). Expressing momentum equations (9) and (10) in terms of these newly defined variables and combining the equations, we have

$$\frac{\partial}{\partial\tau}(m_e\mathbf{U}_e+m_i\mathbf{U}_i)=\frac{e}{c}(\mathbf{U}_i-\mathbf{U}_e)\times\mathbf{B}, \tag{12}$$

where we have used $m_e\nu_{ei}=m_i\nu_{ie}$. Expressing $\mathbf{B}=\hat{e}_xB_0+\hat{e}_zB(x,t)$, the x, y, and z components of Eq. (12) are

$$\frac{\partial u}{\partial\tau}=\frac{eB(x,t)}{(m_e+m_i)c}(U_{iy}-U_{ey}), \tag{13}$$

$$\frac{\partial}{\partial\tau}(m_eU_{ey}+m_iU_{iy})=0, \tag{14}$$

and

$$\frac{\partial v}{\partial\tau}=-\frac{eB_0}{(m_e+m_i)c}(U_{iy}-U_{ey}), \tag{15}$$

respectively. From Eq. (14), it is evident that the total momentum is conserved along the y direction. Taking $U_{ey}(\xi,0)=U_{iy}(\xi,0)=0$, we find

$$U_{iy}=-\frac{m_e}{m_i}U_{ey}. \tag{16}$$

Since the magnetic field associated with the wave under study is along the z direction, i.e., $B(x,t)\hat{e}_z$, the current flows in y direction. This can be further verified from Eq. (6) which is given by

$$ne(U_{iy}-U_{ey})=-\frac{c}{4\pi}\frac{\partial B}{\partial x}. \tag{17}$$

Substituting $(U_{iy}-U_{ey})$ in Eqs. (13) and (15), we obtain

$$\frac{\partial u}{\partial\tau}=-\left[\frac{B}{4\pi(m_e+m_i)n(\xi,0)}\right]\frac{\partial B}{\partial\xi}, \tag{18}$$

$$\frac{\partial v}{\partial\tau}=\left[\frac{B_0}{4\pi(m_e+m_i)n(\xi,0)}\right]\frac{\partial B}{\partial\xi}. \tag{19}$$

The evolution equation for magnetic field can further be expressed by taking curl (z component) in the electron momentum equation (9), and using Eq. (3), we have

$$\left(\frac{\partial}{\partial t}+u\frac{\partial}{\partial x}\right)B+B\frac{\partial u}{\partial x}-B_0\frac{\partial v}{\partial x} = -\frac{cm_e}{e}\frac{\partial}{\partial x}\frac{\partial U_{ey}}{\partial\tau}+\frac{m_ec^2\nu_{ei}}{4\pi e^2}\frac{\partial}{\partial x}\left(\frac{1}{n}\frac{\partial B}{\partial x}\right). \tag{20}$$

In Eq. (17), substituting U_{iy} from Eq. (16), we have

$$\left(1+\frac{m_e}{m_i}\right)U_{ey}=\frac{c}{4\pi en}\frac{\partial B}{\partial x}. \tag{21}$$

Substituting u_{ey} in Eq. (20) (in terms of Lagrangian variable), we have

$$\frac{\partial B}{\partial\tau}+\frac{Bn}{n(\xi,0)}\frac{\partial u}{\partial\xi}-\frac{B_0n}{n(\xi,0)}\frac{\partial v}{\partial\xi} = \frac{c^2}{4\pi e^2}\left(\frac{m_em_i}{m_e+m_i}\right)\frac{n}{n(\xi,0)}\frac{\partial}{\partial\xi}\left[\frac{\partial}{\partial\tau}\left(\frac{1}{n(\xi,0)}\frac{\partial B}{\partial\xi}\right)\right] +\frac{m_ec^2\nu_{ei}}{4\pi e^2}\frac{n}{n(\xi,0)}\frac{\partial}{\partial\xi}\left(\frac{1}{n(\xi,0)}\frac{\partial B}{\partial\xi}\right). \tag{22}$$

Now we normalize Eqs. (8), (18), (19), and (22) by $n\to n/n_0$, $v\to v/v_A$, $B\to B/B_0$, $\xi\to\xi/L$, and $\tau\to\tau v_A/L$, with n_0, v_A, and L denoting a constant equilibrium density, the Alfvén velocity, and an arbitrary length scale, respectively. Then, Eqs. (8), (18), and (22), respectively, become

$$\frac{\partial}{\partial\tau}\left(\frac{1}{n}\right)=\frac{1}{n(\xi,0)}\frac{\partial u}{\partial\xi}, \tag{23}$$

$$\frac{\partial u}{\partial\tau}=-\frac{1}{2n(\xi,0)}\frac{\partial B^2}{\partial\xi}, \tag{24}$$

$$\frac{\partial v}{\partial\tau}=\frac{1}{n(\xi,0)}\frac{\partial B}{\partial\xi}, \tag{25}$$

and

$$\frac{\partial B}{\partial\tau}=-\frac{Bn}{n(\xi,0)}\frac{\partial u}{\partial\xi}+\frac{n}{n(\xi,0)}\frac{\partial v}{\partial\xi}+D\frac{n}{n(\xi,0)} \frac{\partial}{\partial\xi}\frac{\partial}{\partial\tau}\left(\frac{1}{n(\xi,0)}\frac{\partial B}{\partial\xi}\right)+\nu\frac{n}{n(\xi,0)}\frac{\partial}{\partial\xi}\left(\frac{1}{n(\xi,0)}\frac{\partial B}{\partial\xi}\right), \tag{26}$$

where $D=(\delta/L)^2$ is the dispersion parameter arising from electron's finite mass, $\nu=(m_ec^2/4\pi n_0e^2)(\nu_{ei}/Lv_A)$ is the dissipation parameter which arises due to collision, and δ is the skin depth defined by $\delta=(c^2m_em_i/[4\pi(m_e+m_i)n_0e^2])^{1/2}$. Equations (23), (25), and (26) can now be combined together to give the following equation in a more compact form as:

$$\frac{\partial^2}{\partial\tau^2}\left(\frac{B}{n}\right)-\frac{1}{n(\xi,0)}\frac{\partial}{\partial\xi}\left[\frac{1}{n(\xi,0)}\frac{\partial B}{\partial\xi}\right] = \frac{1}{n(\xi,0)}\frac{\partial^2}{\partial\tau\partial\xi}\left[\frac{1}{n(\xi,0)}\frac{\partial}{\partial\xi}\left(D\frac{\partial B}{\partial\tau}+\nu B\right)\right]. \tag{27}$$

Furthermore, Eqs. (23) and (24) can be combined to give

$$\frac{\partial^2}{\partial\tau^2}\left(\frac{1}{n}\right) = -\frac{1}{2n(\xi,0)}\frac{\partial}{\partial\xi}\left(\frac{1}{n(\xi,0)}\frac{\partial B^2}{\partial\xi}\right). \tag{28}$$

These two coupled nonlinear partial differential equations (27) and (28) are the governing equations that describe the dynamics of the nonlinear, dispersive Alfvén wave in an electron-ion plasma. It is to be noted that the above model is appropriate for low-dense plasma as the analysis is valid for $(v_A/c) \le D \ll (m_e/m_i)$, i.e., for small dispersion parameter D and Alfvén velocity v_A.

Before going to the details of the nonlinear analysis, let us linearize equations (27) and (28) by assuming $n = 1 + \tilde{n}$ and $B = \tilde{b}$, and obtain the following linear equation:

$$\left(\frac{\partial^2}{\partial\tau^2} - \frac{\partial^2}{\partial\xi^2}\right)\tilde{b} = D\frac{\partial^4\tilde{b}}{\partial^2\tau\partial^2\xi} + \nu\frac{\partial^3\tilde{b}}{\partial\tau\partial^3\xi}. \tag{29}$$

Then, assuming the solution in the form of Fourier mode $\tilde{b} \sim \exp[-i(\omega\tau - k\xi)]$ (where ω and k are the oscillation frequency and wave number), we obtain the following dispersion relation for the linear Alfvén wave:

$$(1 + Dk^2)\,\omega^2 + i\nu k^2\omega - k^2 = 0, \tag{30}$$

where the collisional parameter ν represents the usual wave damping. In absence of collision the above dispersion relation (in dimensional unit) becomes

$$\omega = \frac{kv_A}{\sqrt{1 + k^2\delta^2}}. \tag{31}$$

This dispersion relation clearly shows that the Alfvén wave is dispersive because of the term δ which arises due to the finite electron inertia. Thus, finite electron mass effect acts as a source of dispersion of the Alfvén wave in electron-ion plasma. More general linear dispersion relation including kinetic pressure terms obtained in Ref. 39 can be reduced to the above dispersion relation [Eq. (31)] in the simplifying limit.

III. NONLINEAR ALFVÉN WAVE

To write the nonlinear system (Eqs. (27) and (28)) in a simplified form, we adopt the Lagrangian mass variable technique.[25] For this, let us define the following new Lagrangian mass variable ζ instead of ξ

$$\zeta = \int^{\xi} n(\xi', 0)d\xi'$$

which yields the mathematical operator

$$\frac{\partial}{\partial\zeta} = \frac{1}{n(\xi,0)}\frac{\partial}{\partial\xi}.$$

Moreover, for convenience, we introduce the specific volume $V(\zeta,\tau) = 1/n(\zeta,\tau)$ [which is the Jacobian of the transformation from (x, t) to (ζ, τ)]. Then, introducing this new mass variable ζ, from Eqs. (27) and (28), we obtain the following simplified couple equations:

$$\frac{\partial^2}{\partial\tau^2}(BV) - \frac{\partial^2 B}{\partial\zeta^2} = \frac{\partial^2}{\partial\zeta^2}\left[D\frac{\partial^2 B}{\partial\tau^2} + \nu\frac{\partial B}{\partial\tau}\right], \tag{32}$$

$$\frac{\partial^2 V}{\partial\tau^2} = -\frac{1}{2}\frac{\partial^2 B^2}{\partial\zeta^2}. \tag{33}$$

These Equations (32) and (33) are complicated nonlinear equations and it is difficult to find an exact analytical solution with its full nonlinearity. Therefore, in Section III A, we will investigate the finite amplitude nonlinear solutions keeping up to third order nonlinear term.

A. Weak amplitude nonlinear wave

To study the dynamics of the finite amplitude nonlinear Alfvén wave, we write

$$V = 1 + \tilde{V} \quad \text{and} \quad B = \tilde{b} \quad \text{with} \quad |\tilde{V}|, |\tilde{b}| < 1.$$

Now, substituting and keeping up to second order term, from Eq. (32), we obtain

$$\frac{\partial^2\tilde{b}}{\partial\tau^2} - \frac{\partial^2\tilde{b}}{\partial\zeta^2} = D\frac{\partial^2}{\partial\tau^2}\left(\frac{\partial^2\tilde{b}}{\partial\zeta^2}\right) + \nu\frac{\partial}{\partial\tau}\left(\frac{\partial^2\tilde{b}}{\partial\zeta^2}\right) - \frac{\partial^2(\tilde{V}\tilde{b})}{\partial\tau^2}. \tag{34}$$

The LHS of the above equation represents linear Alfvén wave whereas the RHS implicates that the wave is modified by dispersion dissipation and nonlinearity. Therefore, this equation shows the wave steepening by nonlinearity, wave spreading by dispersion, and amplitude modulation by dissipation. These three physical phenomena can lead to the well know evolution equation for finite amplitude Alfvén Wave.

Moreover, the small amplitude nonlinear wave equations are derived by assuming that the equilibrium density is homogeneous, i.e., $n(\xi, 0) = 1$, therefore $\zeta = \xi\,[\equiv x - \int v(\xi,\tau')d\tau']$. Also, in this weak amplitude limit, $\xi(\zeta) \equiv x$ and $\tau \equiv t$ (actually in this case, $\xi(\zeta)$ and τ are no longer remain Lagrangian variables but become equivalent to x and t). Therefore, we rewrite the above Equation (34) in the following form:

$$\left(\frac{\partial}{\partial t} - \frac{\partial}{\partial x}\right)\left(\frac{\partial}{\partial t} + \frac{\partial}{\partial x}\right)\tilde{b} = D\frac{\partial^2}{\partial t^2}\left(\frac{\partial^2\tilde{b}}{\partial x^2}\right) + \nu\frac{\partial}{\partial t}\left(\frac{\partial^2\tilde{b}}{\partial x^2}\right) - \frac{\partial^2}{\partial t^2}(\tilde{V}\tilde{b}). \tag{35}$$

Also in absence of dissipation and for negligible dispersion ($D \ll 1$), the linear equation (29) can be expressed as

$$\left(\frac{\partial}{\partial t} - \frac{\partial}{\partial x}\right)\left(\frac{\partial}{\partial t} + \frac{\partial}{\partial x}\right)\tilde{b} = 0. \tag{36}$$

For the Alfvén wave propagating in the positive x direction only, from the above relation, we get

$$\frac{\partial}{\partial t} = -\frac{\partial}{\partial x}$$

and this approximation yields (from Eq. (33))

$$\tilde{V} \approx -\frac{\tilde{b}^2}{2}.$$

Then, substituting all these in Eq. (35) and integrating the transformed equation once with the boundary condition at $x \to \infty$, $\tilde{b} \to 0$, we obtain

$$\frac{\partial \tilde{b}}{\partial t} + \left[1 + \frac{3}{4}\tilde{b}^2\right]\frac{\partial \tilde{b}}{\partial x} + \frac{D}{2}\frac{\partial^3 \tilde{b}}{\partial x^3} = \frac{\nu}{2}\frac{\partial^2 \tilde{b}}{\partial x^2}. \tag{37}$$

Finally, a further transformation of coordinates

$$\hat{x} = x - t \quad \text{and} \quad \hat{t} = t$$

renders the following usual form of the modified Korteweg-de Vries Burgers (mKdVB) equation with $\tilde{b} \equiv \phi$

$$\frac{\partial \phi}{\partial \hat{t}} + \frac{3}{4}\phi^2\frac{\partial \phi}{\partial \hat{x}} + \frac{D}{2}\frac{\partial^3 \phi}{\partial \hat{x}^3} = \frac{\nu}{2}\frac{\partial^2 \phi}{\partial \hat{x}^2}. \tag{38}$$

For a collisionless plasma $\nu = 0$, the above equation can be reduced to modified Korteweg-de Vries (mKdV) equation.

It is to be noted that the nonlinear equation (38) under investigation can also be obtained by the well known reductive perturbation technique. Interestingly, here, keeping only up to second order terms of the dynamical variable, we obtain the same equation from arbitrary nonlinear equation formulated in Lagrangian variables.

B. Moving-frame nonlinear analysis

In this section, we present an exact solution of Eq. (38) in a frame moving with the phase velocity of the wave. We hope that this will improve our understanding on the behavior of the nonlinear system [Eq. (38)]. To investigate the nonlinear solution, we transform equation (38) to the moving frame $\chi = M\hat{t} - \hat{x}$, where M is the Mach number (normalized phase velocity). Then, integrating the transformed equation once subject to the boundary conditions $\phi \to 0$, all derivatives $\to 0$ as $\chi \to \infty$, and we finally obtain the following nonlinear ordinary differential equation:

$$D\frac{d^2\phi}{d\chi^2} + \frac{\phi^3}{2} - 2M\phi + \nu\frac{d\phi}{d\chi} = 0. \tag{39}$$

Then, we recast this nonlinear equation (39) in the following two simultaneous equations:

$$\begin{aligned} \frac{d\phi}{d\chi} &= \psi, \\ \frac{d\psi}{d\chi} &= -\frac{\nu}{D}\psi + \frac{\phi}{D}\left[2M - \frac{\phi^2}{2}\right]. \end{aligned} \tag{40}$$

In the $\phi - \psi$ plane, this dynamical system has the following two physically possible equilibrium (stationary) points:

$$(0,0) \text{ and } (\phi^* \equiv 2\sqrt{M},\ 0).$$

To investigate the nature of these two stationary points, we consider the two cases of interest: collisionless and collisional.

In the collisionless case, we neglect the electron-ion collision ($\nu = 0$) in Eq. (39) [i.e., in Eq. (40)] and calculate the variational matrix of the system (40) at these two stationary points. These matrices are as follows:

$$J_{(0,0)} = \begin{bmatrix} 0 & 1 \\ \frac{2M}{D} & 0 \end{bmatrix}, \quad J_{(\phi^*,0)} = \begin{bmatrix} 0 & 1 \\ -\frac{4M}{D} & 0 \end{bmatrix}. \tag{41}$$

The corresponding pair of eigen values are determined from the following characteristic (quadratic) equations:

$$\lambda^2 - \frac{2M}{D} = 0 \quad \text{and} \quad \Lambda^2 + \frac{4M}{D} = 0. \tag{42}$$

These two characteristic equations determine the pair of eigen values as $\pm\sqrt{2M/D}$ (real and distinct) and $\pm i\,2\sqrt{M/D}$ (purely imaginary), respectively. This implies that the stationary point (0, 0) is a saddle point and the stationary point $(\phi^*, 0)$ is a center. In case of saddle point (left panel of Fig. 1 shows that a small perturbation in the neighborhood of this point forms a homoclinic orbit, i.e., separetrix in the $\phi - \psi$ phase-space which is the signature of the soliton solution), Equation (38) (with $\nu = 0$) is analytically solvable, and the analytical solution gives the following single soliton solution:

$$\phi(x,t) = 2\sqrt{2M}\,\mathrm{sech}\left[\sqrt{\frac{2M}{D}}\chi\right]. \tag{43}$$

This shows that the width of the soliton $(\propto\sqrt{D})$ depends on the electron inertia induced dispersion. Moreover, the numerical solution of Equation (38) with $\nu = 0$ is also provided in Sec. V.

Next, we consider the collisional case and calculate the variational matrix of the system (40) at these two stationary points. These matrices are as follows:

$$J_{(0,0)} = \begin{bmatrix} 0 & 1 \\ \frac{2M}{D} & -\frac{\nu}{D} \end{bmatrix}, \quad J_{(\phi^*,0)} = \begin{bmatrix} 0 & 1 \\ -\frac{4M}{D} & -\frac{\nu}{D} \end{bmatrix}. \tag{44}$$

The corresponding pair of eigen values are determined from the following characteristic (quadratic) equations:

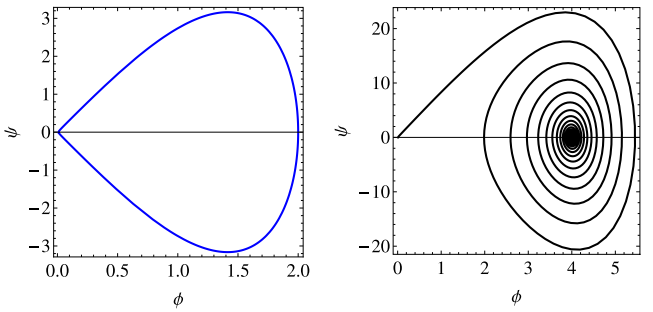

FIG. 1. Phase-space trajectories in the $\phi - \psi$ plane of the dynamical system. The left figure (blue solid curve) is drawn for $M = 0.5$ and the right figure (black solid curve) is drawn for $M = 4$.

$$\lambda^2 + \left(\frac{\nu}{D}\right)\lambda - \frac{2M}{D} = 0,$$
$$\Lambda^2 + \left(\frac{\nu}{D}\right)\Lambda + \frac{4M}{D} = 0. \tag{45}$$

These two characteristic equations determine the following eigen values for the stationary points (0, 0) and $(\phi^*, 0)$, respectively

$$\lambda_{(0,0)} = \frac{1}{2D}\left[-\nu \pm \sqrt{\nu^2 + 8DM}\right] \tag{46}$$

and

$$\Lambda_{(\phi^*,0)} = \frac{1}{2D}\left[-\nu \pm \sqrt{\nu^2 - 16DM}\right]. \tag{47}$$

The eigen values (46) corresponding to the stationary point (0, 0) are real and distinct, which indicate that the stationary point (0, 0) is a saddle point. The eigen values (47) corresponding to the stationary point $(\phi^*, 0)$ are either pair of complex conjugate with negative real part or real (and distinct) with negative sign according as

$$\nu \lessgtr 4\sqrt{DM}. \tag{48}$$

Thus, the stationary point $(\phi^*, 0)$ is either stable focus or stable node. In this collisional case, right panel of Fig. 1 shows that a small perturbation in the vicinity of the point (0, 0) forms a heteroclinic orbit between this point and the point $(\phi^*, 0)$, which is the signature of the shocklike structures. However, in this collisional case, Equation (38) is not exactly analytically solvable as its Hamiltonian is not conserved. Therefore to get the insight of the solutions, we numerically simulate this Equation (38), and the results are shown graphically in Sec. V.

IV. WAVE MODULATION FOR SMALL WAVE NUMBER: NONLINEAR SCHRÖDINGER EQUATION

In Section III, we do not consider the effects of self-interaction of the Alfvén wave (an intrinsic character of nonlinear wave propagation) that introduces self-focusing effect (modulational instability) in the system. In this section, we consider this effect for the nonlinear Alfvén wave in the presence of electron-ion collision induced dissipation in the long-wavelength limit. The nonlinear Schrödinger equation (NLSE) with cubic nonlinearity clearly explains such self-interaction effects.[40] Moreover, it is well-known from different physical systems[41–43] that the classical KdV as well as the extended KdV equations can easily be transformed to the NLSE in the long-wavelength limit. Therefore, to study the modulational instability (self-interaction effect) of nonlinear Alfvén waves in the presence of dissipation, we derive the NLSE from the above nonlinear mKdVB equation (38) in the long-wave length limit. To achieve this, we introduce the following stretched variable ξ and τ:

$$\hat{\xi} = \epsilon(\hat{x} - U_g\hat{t}) \quad \text{and} \quad \hat{\tau} = \epsilon^2\hat{t}, \tag{49}$$

where U_g is the group velocity of the wave and expands the wave amplitude ϕ in the following way:

$$\phi(\hat{x}, \hat{t}) = \sum_{j=1}^{\infty} \epsilon^j \sum_{l=-\infty}^{\infty} \phi_l^{(j)}(\hat{\xi}, \hat{\tau}) \exp\left[i(k\hat{x} - \omega\hat{t})l\right] \tag{50}$$

with the reality condition $\phi_{-l}^{(j)} = (\phi_l^{(j)})^*$. Also to incorporate the weak collisional effects and for consistent perturbarion, we consider the following scaling:

$$\nu \sim O(\epsilon^2). \tag{51}$$

Now using (49)–(51) in Equation (38), in the lowest order with $l = \pm 1$, we obtain the dispersion relation

$$\omega = -\frac{D}{2}k^3. \tag{52}$$

The second order terms with $l = \pm 1$ give the following compatibility condition:

$$U_g = -\frac{3}{2}Dk^2 \equiv \frac{d\omega}{dk}. \tag{53}$$

Finally, we substitute the above derived equations into third order $(n = 3)$ equations and obtain the following damped nonlinear Schrödinger equation (NLSE) for $\phi_1^{(1)}[\equiv\phi]$:

$$i\frac{\partial\phi}{\partial\hat{\tau}} + P\frac{\partial^2\phi}{\partial\hat{\xi}^2} + Q|\phi|^2\phi + i\gamma\phi = 0. \tag{54}$$

In this equation, the group dispersion coefficient

$$P = -\frac{3}{2}Dk \equiv \frac{1}{2}\frac{d^2\omega(k)}{dk^2} \tag{55}$$

is related to the curvature of the dispersion relation $\omega(k)$ [Eq. (52)], which is always negative for all wave number k. The coefficient of nonlinear term

$$Q = -\frac{3}{4}k \tag{56}$$

is related to the nonlinear frequency shift. The dissipative term

$$\gamma = \frac{\nu k^2}{2} \tag{57}$$

is related to the electron-ion collision.

A. Modulational instability in the presence of electron-ion collision

Now, we analyze the stability of the above NLSE (54) for very low-frequency Alfvén waves in the presence of dissipation. In this NLSE [Eq. (54)], the term $-Q|\phi|^2$ plays the role of a potential energy. The local maxima of this potential energy act as an effective potential well in the plasma. The high frequency waves reflect from the regions of high density, and the amplitude-dependent ponderomotive force forms a low-density region (cavity). As a consequence, the low-frequency waves become trapped within these density depleted regions, and the wave energy will concentrate at the bottom of the well. The energy concentration makes the well

deeper by making this energy even larger. Thus, the formation of the cavity is an unstable physical process that occurs due to the energy localization in the medium. This process is known as modulational instability.[40,44–46] Here, we investigate this instability for nonlinear Alfvén waves in the presence of electron-ion collision.

For this purpose, we assume that in the presence of collision, the amplitude evolution equation (54) possesses the following plane wave solution:

$$\phi = \phi_0(\hat{\tau}) \exp\left(-i\int_0^{\hat{\tau}} \Delta(\tau')d\tau'\right), \tag{58}$$

where $\phi_0(\hat{\tau})$ and $\Delta(\hat{\tau})$ are the amplitude of the pump carrier wave and the nonlinear frequency shift in the presence of dissipation. Substituting this solution (58) in Equation (54), we obtain the following two equations:

$$\frac{d\phi_0}{d\hat{\tau}} + \gamma\phi_0 = 0 \Rightarrow \phi_0(\hat{\tau}) = \phi_{00}\exp(-\gamma\hat{\tau}) \text{ and}$$
$$\Delta(\hat{\tau}) = -Q|\phi_0(\hat{\tau})|^2 = -Q|\phi_{00}|^2\exp(-2\gamma\hat{\tau}), \tag{59}$$

where ϕ_{00} is a real constant. Also note that $\phi_0(\hat{\tau}) \to 0$ as $\hat{\tau} \to \infty$, which implies that ϕ_0 is bounded and stable. Therefore, for stability analysis, we consider the perturbation about this stable solution in the following standard procedure:

$$\phi = [\phi_0(\hat{\tau}) + \tilde{\phi}(\hat{\xi},\hat{\tau})]\exp\left(-i\int_0^{\hat{\tau}} \Delta(\tau')d\tau'\right), \tag{60}$$

where $\tilde{\phi}(|\tilde{\phi}| \ll \phi_0)$ is the perturbed amplitude of the modulated wave. Then, substituting this Equation (60) in Equation (54), we obtain the following linearized two coupled equations:

$$\frac{\partial\tilde{\phi}_I}{\partial\hat{\tau}} = P\frac{\partial^2\tilde{\phi}_R}{\partial\hat{\xi}^2} + 2Q|\phi_0|^2\tilde{\phi}_R - \gamma\tilde{\phi}_I \text{ and}$$
$$\frac{\partial\tilde{\phi}_R}{\partial\hat{\tau}} = -P\frac{\partial^2\tilde{\phi}_I}{\partial\hat{\xi}^2} - \gamma\tilde{\phi}_R. \tag{61}$$

Here, $\tilde{\phi} = \tilde{\phi}_R + i\tilde{\phi}_I$, $\phi_{R(I)}$ is the real (imaginary) part of ϕ.

Finally, the space-time dependence of the perturbation of the form $\tilde{\phi} \sim \exp(i\vartheta)$, where $\vartheta(=\tilde{k}\hat{\xi} - \int_0^{\hat{\tau}} \tilde{\omega}(\acute{\tau})d\acute{\tau})$ is the modulated phase, with $\tilde{k}(\ll k)$ and $\tilde{\omega}(\ll\omega)$ are the wave number and modulation frequency, respectively, yield the following dispersion relation:

$$(\tilde{\omega} + i\gamma)^2 = P^2\tilde{k}^4 - 2PQ|\phi_0|^2\tilde{k}^2. \tag{62}$$

This shows that the electron-ion collision provides the usual damping. Also, the system is stable for $PQ < 0$. However, there is a possibility of the instability if $PQ > 0$ (both P and Q are of same sign: here both P and Q are negative for all $\tilde{k}$ [Eqs. (55) and (56)]). Thus, the instability occurs if

$$\tilde{k}^2 < \tilde{k}_{cr}^2 = \left(\frac{2Q}{P}\right)|\phi_0|^2 = \left(\frac{1}{D}\right)|\phi_{00}|^2\exp(-2\gamma\hat{\tau}) \tag{63}$$

provided with this values of $\tilde{k}$, the following inequality must holds:

$$\gamma < \sqrt{P^2\tilde{k}^4\left(\frac{\tilde{k}_{cr}^2}{\tilde{k}^2} - 1\right)}. \tag{64}$$

This determines the maximum time τ_{max} to observe instability

$$\tau_{max} = \frac{1}{2\gamma}\ln\left(\frac{2PQ\tilde{k}^2|\phi_{00}|^2}{\gamma^2 + P^2\tilde{k}^4}\right)$$
$$= \left(\frac{1}{\nu k^2}\right)\ln\left(\frac{18D\tilde{k}^2|\phi_{00}|^2}{k^2\nu^2 + 18D^2\tilde{k}^4}\right). \tag{65}$$

Thus, the instability growth will cease for $\hat{\tau} \geq \tau_{max}$. Now, by setting $\tilde{\omega} = i\Gamma$, the dispersion relation for the instability growth rate becomes

$$(\Gamma + \gamma)^2 = 2PQ|\phi_0|^2\tilde{k}^2 - P^2\tilde{k}^4. \tag{66}$$

The maximum growth rate is found by taking the derivative of Eq. (66) with respect to $\tilde{k}^2$, and setting this to zero, we have

$$\tilde{k}_{max}^2 = \left(\frac{Q}{P}\right)|\phi_0|^2 = \left(\frac{1}{2D}\right)|\phi_{00}|^2\exp(-2\gamma\hat{\tau}) \tag{67}$$

which is just half of the $\tilde{k}_{cr}$ value. With this value of $\tilde{k}_{max}^2$, we can find the maximum growth rate

$$\Gamma_{max} = |Q||\phi_0|^2 - \gamma. \tag{68}$$

Therefore, in the presence of electron-ion collision, the nonlinear Alfvén waves are modulationally unstable when

$$|\phi_0|^2\rangle = \frac{2\,\nu k}{3}.$$

B. Approximate analytical solution: Weakly dissipative envelope (bright) soliton

In the above damped NLSE [Eq. (54)], the group dispersion coefficient P [Eq. (55)] and the nonlinear coefficient Q [Eq. (56)] are all negative for all values of the wave number k. Thus, to find the envelope (bright) soliton of the damped NLSE [Eq. (54)], we recast the equation in the following normal form:

$$i\frac{\partial\phi}{\partial\bar{\tau}} - \frac{1}{2}\frac{\partial^2\phi}{\partial\bar{\xi}^2} - |\phi|^2\phi + i\bar{\gamma}\phi = 0, \tag{69}$$

where $\bar{\tau} = |Q|\hat{\tau}$, $\bar{\xi} = \hat{\xi}\sqrt{|Q|/2|P|}$ and $\bar{\gamma} = \gamma/|Q|$. This equation exhibits bright or envelope soliton. This Equation (69) is solved numerically and the solutions are shown graphically in Fig. 2. However, here we solve this equation analytically.

In absence of dissipation ($\nu = 0 \Rightarrow \bar{\gamma} = 0$), we have the usual NLSE which is an exactly integrable Hamiltonian system, possesses infinite number of conservation. In this case,

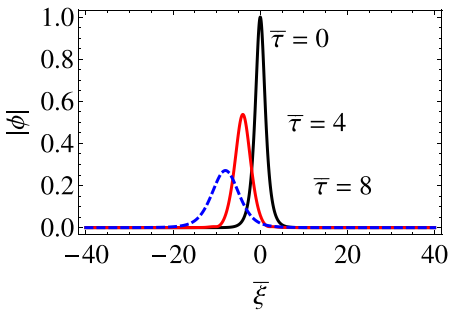

FIG. 2. Time-dependent numerical solution of Equation (69) with $\bar{\gamma} = 0.1$ and initial amplitude $a = 1$.

let us assume a solution of the form $\phi(\bar{\xi}, \bar{\tau}) = \rho(\bar{\xi}, \bar{\tau}) \exp[i\varphi(\bar{\xi}, \bar{\tau})]$ and then solve the ordinary differential equations for φ and ρ subject to the boundary condition $\rho \to 0$ as $\bar{\xi} \to \pm\infty$. We finally obtain the following single envelope (bright) soliton which in terms of actual parameters reads as:

$$\phi(\hat{\xi}, \hat{\tau}) = a\,\mathrm{sech}\left[\frac{a}{2\sqrt{D}}\left(\hat{\xi} + \frac{3}{2}k\sqrt{D}\kappa\hat{\tau}\right)\right] \times \exp\left[\frac{i}{2\sqrt{D}}\left(\kappa\hat{\xi} - \frac{3k}{4}\sqrt{D}(a^2 - \kappa^2)\hat{\tau}\right)\right], \quad (70)$$

where a and κ are two soliton parameters in which a is the amplitude of the soliton. This shows that the disturbances resemble with the soliton shape with an exponential factor making oscillation between a maxima and a minima. The resultant structure is the envelope excitation of nonlinear Alfvén wave.

In the case of weak dissipation (here it is indeed weak as $\nu \sim O(\epsilon^2)$), we can solve the above damped NLSE [Eq. (54)] perturbatively by taking $\varepsilon(\phi)$ as a small perturbed quantity. To apply this perturbation, we consider the general solution of the perturbed soliton is of the following form:[47]

$$\phi(\bar{\xi}, \bar{\tau}) = a(\bar{\tau})\mathrm{sech}\left[a(\bar{\tau})(\bar{\xi} + b(\bar{\tau}))\right] \times \exp\left[i\bar{\xi}\kappa(\bar{\tau}) - i\sigma(\bar{\tau})\right], \quad (71)$$

where a, b, σ, and κ are the soliton parameters. Finally, by applying the conservation laws for the NLSE (conserved integral relations,[47]), we obtain the following bright soliton (envelope soliton) in the presence of dissipation (electron-ion collision), which in terms of actual variable reads as:

$$\phi(\hat{\xi}, \hat{\tau}) = a_0\exp(-2\gamma\hat{\tau})\mathrm{sech}\left[a_0\exp(-2\gamma\hat{\tau})\frac{1}{2\sqrt{D}} \times\left(\hat{\xi} + \frac{3k}{2}\sqrt{D}\kappa_0\hat{\tau}\right)\right]\exp\left\{\frac{i}{2\sqrt{D}}\left[\kappa_0\hat{\xi} + \frac{3k}{4} \times\sqrt{D}\left(\kappa_0^2\hat{\tau} + a_0^2\left(\frac{\exp(-4\gamma\hat{\tau}) - 1}{4\gamma}\right)\right)\right]\right\}, \quad (72)$$

where a_0 and κ_0 are the initial values of a and κ, respectively. In the limit $\gamma \to 0$, we recover the previous result (70) (with $a_0 = a$ and $\kappa_0 = \kappa$). It is clear that as the time elapses, the amplitude of the bright (envelope) soliton decreases exponentially with decay rate $\sim 2\gamma$. The numerical solution in Fig. 2 also shows similar nature. Thus, the electron-ion collisions have damping effect on the bright soliton structure of nonlinear Alfvén waves in electron-ion plasma.

V. NUMERICAL SIMULATION

In this section, we numerically simulate both the nonlinear equations (38) and (54) with the help of the MATHEMATICA.

A. Numerical solutions of modified Korteweg-de Vries Burgers equation

To simulate Equation (38) numerically, first we solve the dynamical system (40) in the absence of collision $\nu = 0$ by the Runge-Kutta-Fehlberg (RKF) method by taking the stationary point (0, 0) as the initial condition with $D = 0.1$. The solutions are shown graphically in Fig. 3. This figure shows that a small perturbation around the equilibrium point (0, 0) (saddle point) develops into a soliton as expected from the analytical solution (43). The comparative study between the figures (left and right) demonstrates that single soliton structure is observed for low Mach number ($M = 0.5$). In case of high Mach number ($M = 3$), single soliton disintegrates into multi-soliton structures with higher amplitude.

Next, we solve the dynamical system (40) by RKF method by taking the stationary point (0, 0) as the initial condition with $D = 0.1$ and $M = 4$. Then, starting from a small perturbation around the initial condition (0, 0) and upon numerical integration of the dynamical system, it is seen that the perturbation develops into a shock-like structure as illustrated in Fig. 4 with oscillating/monotonic transition corresponding to the second stationary point $(\phi^*, 0)$. Actually, if one assumes that for $\chi = -\infty(\hat{x} = \infty)$ the particle was located at $\phi = 0$, then at $\chi = \infty(\hat{x} = -\infty)$, it appears at the point $\phi = \phi^*$ and the solution describes a shocklike structure. The equilibrium point (0, 0) corresponds to the equilibrium downstream state, and the point $(\phi^*, 0)$ corresponds to the upstream state. In case of weak dissipation ($\nu = 0.1$), the dispersion dominates over dissipation and therefore the transition occurs with an oscillating behavior that forms dispersive (oscillatory) shock structure as illustrated in the left figure of Fig. 4. On the other hand for strong dissipation ($\nu = 1$), the dissipation dominates over dispersion, and therefore, the transition occurs with a monotonic behavior that forms monotonic shock structure as illustrated in the right figure of Fig. 4. Thus, according to the condition (48), the stable focus always corresponds to the oscillatory nature,

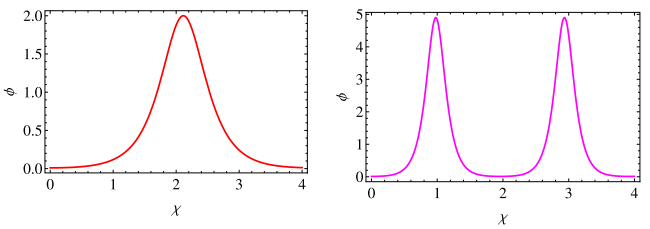

FIG. 3. Numerical solution of the dynamical system (40) in the absence of dissipation ($\nu = 0$) with $D = 0.1$. Formation of single soliton for ϕ (dimensionless magnetic field fluctuations) in the traveling wave frame χ. The left figure (red solid curve) is drawn for $M = 0.5$ and the right figure (magenta solid curve) is drawn for $M = 3$.

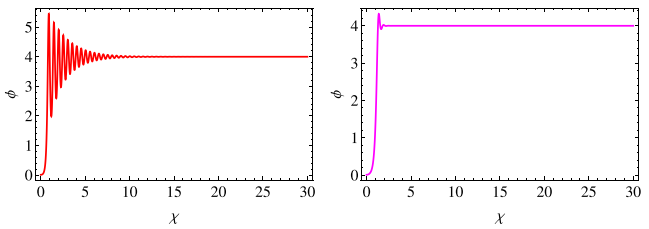

FIG. 4. Numerical solution of the dynamical system (40) in the presence of dissipation ($\nu \neq 0$) with $M = 4$. Formation of shock-like structure for ϕ in the traveling wave frame χ. The left figure (red solid curve) shows oscillatory shock structure for weak dissipation ($\nu = 0.1$). The right figure (magenta solid curve) shows monotonic shock structure for strong dissipation ($\nu = 1$).

whereas the stable node corresponds to the monotonic nature of the solution. In both the cases, the observed shock is compressive in nature. The shock strength (related to the extreme upstream and downstream values) is given by $[\phi(+\infty) - \phi(-\infty) =] \phi^* = 2\sqrt{M}$.

Finally, we solve the dynamical system (40) by the RKF method with the stationary point $(\phi^*, 0)$ as the initial condition with $M = 4$. The simulation results are shown graphically in Fig. 5. This figure illustrated that a small perturbation around this stationary point develops into breather structures.

A breather is a nonlinear wave in which energy concentrates in a localized and oscillatory manner. It is a localized periodic solution of a nonlinear system. A breather is described as an oscillatory solution (wave-packet) about a stationary point whose envelope and oscillatory part move with different velocities.[48] We can see from the simulation that indeed the solutions represented in Fig. 5 resemble the situation of a breather.

B. Numerical solutions of damped nonlinear Schrödinger equation

Here, we numerically simulate the nonlinear equation (69) using MATHEMATICA based finite difference scheme. For the time-dependent numerical solution, we use the envelope (bright) soliton solution as the initial waveform

$$\phi(\bar{\xi}, 0) = a\,\mathrm{sech}\,(a\bar{\xi})\exp(i\bar{\xi}), \quad \bar{\xi} \in [-L, L],$$

where a is the amplitude of the initial waveform and L is approximately the system size. The boundary condition is $\phi(-L, \bar{\tau}) = \phi(L, \bar{\tau})$. To obtain adequate results through computation, we take $L = 40$ and $a = 1$. The time-dependent numerical solutions are shown in Fig. 2. These solutions reveal that the amplitude of the envelope decreases (spatial width increases) with time $\bar{\tau}$ in the presence of dissipation (electron-ion collision). This confirms the weakly dissipative nature of the envelope as obtained by the approximate analytical solution (72). The NLSE possesses another class of nonlinear solution known as rational solutions which play a major role in the theory of rogue waves.[28,30,49] The first-order rational solution of NLSE is known as Peregrine soliton[27] which is localized in both space and time. The solutions are the space-periodic breather[50] and the time-periodic breather[51] type solutions. The Peregrine solitons appear as a bright (i.e., a high peak between two troughs) as well as dark or hole (i.e., an isolated deep trough between two crests) Peregrine soliton depending on the phase of the underlying carrier wave.[27]

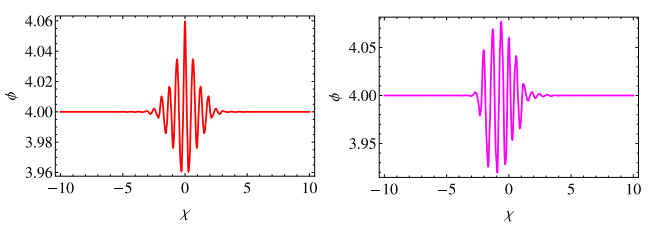

FIG. 5. Breather solution of the dimensionless dynamical system (40) with $M = 4$ and $(\phi^*, 0)$ as the initial condition. The left figure (red solid curve) shows breather structure without dissipation, whereas the right figure (magenta solid curve) shows the same with dissipation ($\nu = 0.1$).

However, here we consider only the formation of dissipative rogue wave, possible breather solution and rogue wave holes. For this initial excitation of the rogue wave in the simulation, based on the soliton solution on a continuous wave background, we consider the following Gaussian-type perturbation pulse as the initial condition:

$$\phi(\bar{\xi}, 0) = \phi_{00} + \epsilon\,\exp\,(-\sigma\bar{\xi}^2), \; \bar{\xi} \in [-L, L], \qquad (73)$$

where ϕ_{00} is the initial plane wave solution of NLSE (which is a non-negative constant), ϵ is a weak modulation amplitude, and σ represents the inverse of the width of initial perturbation pulse. The time-dependent simulation results are shown in Figs. 6 and 7. One can see from the left panel of Fig. 6 that in the absence of dissipation $(\bar{\gamma} = 0)$ at time $\bar{\tau} = 5$, the maximum wave amplitude at $\bar{\xi} = 0$

$$|\phi(\bar{\xi} = 0, \bar{\tau} = 5) - \phi_{00}|_{max} = 0.15$$

exceeds the modulated wave amplitude ($\epsilon = 0.05$) by a factor of three, which is the main characteristic of a bright Peregrine soliton (the localization of wave in both space and time, where the carrier amplitude is amplified by a factor of three).[27]

Then, in the simulation, we introduce the electron-ion collision induced dissipative effects. The simulation result is shown graphically in the right panel of Fig. 6. One can see from this figure that the amplitude of the nonlinear wave decreases in the presence of dissipation, resulting in the formation of dissipative rogue wave.

Further, we have performed numerical simulations of the time evaluation of the localized initial pulse given by

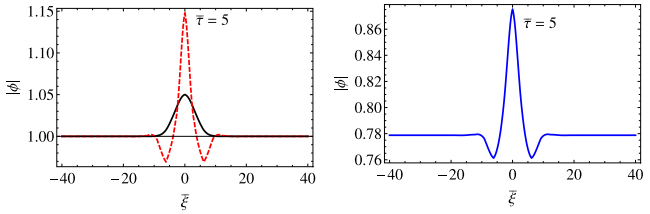

FIG. 6. Time-dependent numerical simulation of Equation (69) with Eq. (73) as the initial condition. The numerical values of the parameters are $\phi_{00} = 1$, $\sigma = 0.05$, and $\epsilon = 0.05$. The left figure is drawn for no dissipation, whereas the right figure is drawn in the presence of dissipation with $\bar{\gamma} = 0.05$. In the left figure, the solid (black) curve is the initial perturbation pulse, and the dotted curve (red) represents the typical profile of a bright Peregrine soliton at $\bar{\tau} = 5$. The right figure represents the same in the presence of dissipation.

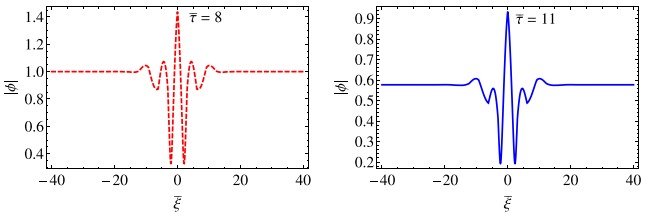

FIG. 7. Typical profiles of breathers. The left figure (red dashed) represents the breather profile in the absence of dissipation at time $\bar{\tau} = 8$. The right figure (blue solid) represents the same profile in the presence of dissipation with $\bar{\gamma} = 0.05$ at time $\bar{\tau} = 11$. The initial condition is same as in Fig. 6.

Eq. (73) at time $\bar{\tau} = 8$ (in the absence of dissipation) and $\bar{\tau} = 11$ (in the presence of dissipation). The results are summarized in Fig. 7, which reveals the characteristic behavior of the localized breathing soliton. The left panel of Fig. 7 demonstrates that the maximum amplitude of the breather is eight times to that of the initial modulation wave amplitude in the absence of dissipation. We can see from the right panel of Fig. 7 that the dissipation present in the system lowers the amplitude of the continuous wave background as well as the nonlinear wave as mentioned in Eq. (59). Thus, the observed breathers are indeed giant breathers, and the collision introduces the usual damping.

Then, in order to excite hole Peregrine soliton, we have performed numerical simulations taking $\epsilon = -0.05$ in the initial perturbation pulse given by Eq. (73). The simulation results are shown in Fig. 8. One can see from the left panel of Fig. 8 that in the absence of dissipation $(\bar{\nu} = 0)$ at time $\bar{\tau} = 5$, the maximum amplitude of hole at $\bar{\xi} = 0$

$$|\phi(\bar{\xi} = 0, \bar{\tau} = 5) - \phi_{00}|_{max} = 0.12$$

exceeds twice the modulated wave amplitude $(|\epsilon| = 0.05)$, which satisfies the characteristics of a hole Peregrine soliton (the localized soliton in both space and time, where the amplification factor of the carrier amplitude is greater than twice the modulated wave amplitude).[36] In the presence of dissipation rogue wave, holes with smaller amplitude are observed as shown in the right panel of Fig. 8.

VI. DISCUSSION

In this work, we have investigated the nonlinear dynamics of the linear-polarized, parallel propagating dispersive Alfvén wave. The electron inertia together with ion inertia introduces the dispersive character of the parallel-propagating Alfvén wave in the electron-ion plasma. This finding is unlike the case investigated earlier where the electron mass is neglected,[9] which turns out to be the source of dispersion. We have also shown that the dynamics of the weakly nonlinear shear Alfvén wave is governed by an mKdV Burgers equation. The Burgers term which is responsible for the generation of shock arises due to the electron-ion collision. This nonlinear equation is analyzed by means of analytic and computation. The numerical results predict the formation of both oscillatory (dispersive) shock for weak dissipation and monotonic shock for strong dissipation. Also, numerical solution predicts the breather-like structures of nonlinear shear Alfvén wave.

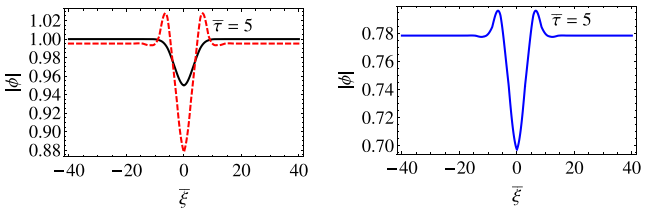

FIG. 8. Time-dependent numerical simulation of Equation (69) with Eq. (73) as the initial condition. The numerical values of the parameters are $\phi_{00} = 1$, $\sigma = 0.05$, and $\epsilon = -0.05$. The left figure is drawn for no dissipation, whereas the right figure is drawn in the presence of dissipation with $\bar{\gamma} = 0.05$. In the left figure, the solid (black) curve is the initial perturbation pulse, and the dotted curve (red) represents the typical profile of a dark or hole Peregrine soliton at $\bar{\tau} = 5$. The right figure represents the same in the presence of dissipation.

We have also investigated the wave modulation characteristics of the nonlinear shear Alfvén wave in the long wavelength limit. Our investigation shows that there is a possibility of the trapping of Alfvén wave in a hole created by the wave itself in the medium, and the dynamics of this modulated wave is governed by a damped NLSE in which the damping is proportional to the electron-ion collision. The analytical and numerical simulations reveal that this modulated wave exhibits weakly dissipative bright (envelope) solitons. Numerical simulation of the damped NLSE also predicts the formation of localized (both space and time: short-lived) large amplitude nonlinear structures known as rogue waves or freak waves, giant breathers, and rogue wave holes.

The magnetic field plays a decisive role in the dynamics of inter stellar molecular clouds and the star formation process.[52] This process belongs to the MHD regime, characterized by highly supersonic, strongly magnetized compressible medium, where self-gravity overpowers the thermal pressure over a wide range of scales.[52] The supersonic motion that is observed in molecular clouds might arise from the Alfvén type MHD waves which have $B_\perp/B_0 = v_\perp/v_A$, perpendicular to the mean magnetic field B_0. The numerical simulation predicts that the magnetic field significantly reduces the rate of star formation, i.e., delays the process. In the present investigation, the observed shocks are compressive in nature with sufficient magnetic field enhancement in the upstream side of the shock. Thus, one can predict that generation of such strong magnetic field can be a potential mechanism to restrict the collapse of molecular clouds due to self-gravity.

The magnetic filed energy grows with the passing of the shock, and the saturation occurs at the upstream side (here the saturation value is $2\sqrt{M}$). After the saturation, the energy stored in the magnetic field is transferred back to the plasma particles, leading to the strong plasma heating and the high energy particles. These high-energy particles are responsible for the particle acceleration mechanism. Thus, the result of the present investigation could be useful for understanding the observed physical phenomena such as particle energization[5,53] and plasma heating.[7]

Moreover, the short-lived large-amplitude magnetic structures are commonly observed in space plasmas. In the upstream of the quasi-parallel bow shock, such short-lived large amplitude pulsations with strong amplitude magnetic

field enhancement have been observed.[54–56] Thus, the observation of Alfvénic rogue waves, giant breathers, and rogue wave holes in the present work could be a viable process to observe short-lived large amplitude excitations in the space plasma.

[1]H. Alfvén, Nature (London) **150**, 405 (1942).
[2]H. L. Pecseli, *Waves and Oscillations in Plasmas* (CRC Press, 2012).
[3]B. Buti, V. L. Galinski, V. I. Shevchenko, G. Lakhina, B. T. Tsurutani, B. E. Goldstein, P. Diamond, and M. V. Medvedev, Astrophys. J. **523**, 849 (1999).
[4]N. F. Cramer, *The Physics of Alfvén Waves* (WILEY-VCH, Germany, 2001).
[5]D. J. Wu and L. Yang, Astron. Astrophys. **452**, L7 (2006).
[6]R. A. López, F. A. Asenjo, V. Muñoz, C.-L. C. Abraham, and J. A. Valdivia, Phys. Rev. E **88**, 023105 (2013).
[7]M. N. Rosenbluth and P. H. Rutherford, Phys. Rev. Lett. **34**, 1428 (1975).
[8]L. Stenflo, A. B. Shvartsburg, and J. Weiland, Phys. Lett. A **225**, 113 (1997).
[9]C. F. Kennel, B. Buti, T. Hada, and R. Pellat, Phys. Fluids **31**, 1949 (1988).
[10]E. Mjolhus, J. Plasma Phys. **19**, 437 (1978).
[11]A. W. Hood, D. González-Delgado, and J. Ireland, Astron. Astrophys. **324**, 11 (1997).
[12]I. De. Moortel, A. W. Hood, J. Ireland, and T. D. Arber, Astron. Astrophys. **346**, 641 (1999).
[13]J. Heyvaerts and E. R. Priest, Astron. Astrophys. **117**, 220 (1983).
[14]T. A. Carter, B. Brugman, P. Pribyl, and W. Lybarger, Phys. Rev. Lett. **96**, 155001 (2006).
[15]S. Dorfman and T. A. Carter, Phys. Rev. Lett. **110**, 195001 (2013).
[16]A. Panwar, H. Rizvi, and C. M. Ryu, Phys. Plasmas **20**, 052103 (2013).
[17]A. Panwar, H. Rizvi, and C. M. Ryu, Phys. Plasmas **20**, 082101 (2013).
[18]Y. Lin, J. R. Johnson, and X. Wang, Phys. Rev. Lett. **109**, 125003 (2012).
[19]J. S. Zhao, Y. Voitenko, D. J. Wu, and J. D. Keyser, Astrophys. J. **785**, 139 (2014).
[20]J. S. Zhao, Y. Voitenko, J. D. Keyser, and D. J. Wu, Astrophys. J. **799**, 222 (2015).
[21]M. L. Rinawa, N. Gaur, and R. P. Sharma, Phys. Plasmas **22**, 022310 (2015).
[22]D. Laveder, T. Passot, P. Sulem, and G. Sanchez-Arriagab, Phys. Lett. A **375**, 3997 (2011).
[23]J. M. Dawson, Phys. Rev. **113**, 383 (1959).
[24]R. C. Davidson, *Methods in Nonlinear Plasma Theory* (Academic, New York, 1972).
[25]H. Schamel, Phys. Rep. **392**, 279 (2004).
[26]N. Chakrabarti, C. Maity, and H. Schamel, Phys. Rev. E **88**, 023102 (2013).
[27]D. H. Peregrine, J. Aust. Math. Soc. Ser. B: Appl. Math. **25**, 16 (1983).
[28]N. Akhmediev and A. Ankiewicz, *Solitons, Nonlinear Pulses and Beams* (Chapman and Hall, London, 1997).
[29]V. E. Zakharov, A. I. Dyachenko, and A. O. Prokofiev, Eur. J. Mech. B/Fluids **25**, 677 (2006).
[30]N. Akhmediev, A. Ankiewicz, and J. M. Soto-Crespo, Phys. Rev. E **80**, 026601 (2009).
[31]G. Yang, Y. Wang, Z. Qin, B. A. Malomed, D. Mihalache, and L. Li, Phys. Rev. E **90**, 062909 (2014).
[32]K. Hammani, B. Kibler, C. Finot, P. Morin, J. F. J. M. Dudley, and G. Millot, Opt. Lett. **36**, 112 (2011).
[33]A. Chabchoub, N. P. Hoffmann, and N. Akhmediev, Phys. Rev. Lett. **106**, 0204502 (2011).
[34]A. Chabchoub, N. Akhmediev, and N. P. Hoffmann, Phys. Rev. E **86**, 016311 (2012).
[35]H. Bailung, S. K. Sharma, and Y. Nakamura, Phys. Rev. Lett. **107**, 0255005 (2011).
[36]A. Chabchoub, S. Neumann, N. P. Hoffmann, and N. Akhmediev, J. Geophys. Res. **117**, C00J02, doi:10.1029/2011JC007671 (2012).
[37]S. K. Sharma and H. Bailung, J. Geophys. Res. **118**, 919, doi:10.1002/jgra.50111 (2013).
[38]A. Sarkar, N. Chakrabarti, and H. Schamel, Phys. Plasmas **22**, 072307 (2015).
[39]J. Zhao, Phys. Plasmas **22**, 042115 (2015).
[40]M. J. Ablowitz and H. Suger, *Solitons and the Inverse Scattereing Transform* (Society for Industrial and Applied Mathematics (SIAM), Philadelphia, 1981).
[41]M. Saito, S. Watanabe, and H. Tanaka, J. Phys. Soc. Jpn. **53**, 2304 (1984).
[42]V. E. Zakharov and E. A. Kuznetsov, Physica D **18**, 455 (1986).
[43]E. J. Parkes, J. Phys. A **20**, 2025 (1987).
[44]O. Bang, W. Krolikowski, J. Wyller, and J. J. Rasmussen, Phys. Rev. E **66**, 046619 (2002).
[45]W. Krolikowski, O. Bang, J. J. Rasmussen, and J. Wyller, Phys. Rev. E **64**, 016612 (2001).
[46]S. Ghosh, S. Sarkar, M. Khan, and M. R. Gupta, Phys. Rev. E **84**, 066401 (2011).
[47]Y. S. Kivshar and G. P. Agarwal, *Optical Solitons-From Fibres to Photonic Crystals* (Academic Press, San Diego, 1995).
[48]G. L. Lamb, *Elements of Soliton Theory* (Wiley, New York, 1980).
[49]K. B. Dysthe and K. Trulsen, Phys. Scr. **T82**, 48 (1999).
[50]N. N. Akhmediev, V. M. Eleonskii, and N. Kulagin, Theor. Math. Phys. (USSR) **72**, 809 (1987).
[51]Y. C. Ma, Stud. Appl. Math. **60**, 43 (1979).
[52]E. C. Ostriker, J. M. Stone, and C. F. Gammie, Astrophys. J. **546**, 980 (2001).
[53]J. R. Wygant, A. Keiling, C. A. Cattell, R. L. Lysak, M. Temerin, F. S. Mozer, C. A. Kletzing, J. D. Scudder, V. Streltsov, W. Lotko, and C. T. Russell, J. Geophys. Res. **107**, 24, doi:10.1029/2001JA900113 (2002).
[54]S. J. Schwartz and D. Burgess, Geophys. Res. Lett. **18**, 373, doi:10.1029/91GL00138 (1991).
[55]S. J. Schwartz, D. Burgess, W. P. Wilkinson, R. L. Kessel, M. Dunlop, and H. Luhr, J. Geophys. Res. **97**, 4209, doi:10.1029/91JA02581 (1992).
[56]D. Burgess, Adv. Space Res. **20**, 673 (1997).